NEOPLASIA
www.neoplasia.com

Volume 13 Number 11 November 2011 pp. 1026–1034 1026

Disclosure of Erlotinib as a Multikinase Inhibitor in Pancreatic Ductal Adenocarcinoma[1,2]

Laura Conradt*, Klaus Godl†, Christoph Schaab†, Andreas Tebbe†, Stefan Eser*, Sandra Diersch*, Christoph W. Michalski‡, Jörg Kleeff‡, Angelika Schnieke§, Roland M. Schmid*, Dieter Saur*,3 and Günter Schneider*,3

*II. Medizinische Klinik, Klinikum rechts der Isar, Technische Universität München, München, Germany; †KINAXO Biotechnologies GmbH, Martinsried, Germany; ‡Chirurgische Klinik, Klinikum rechts der Isar, Technische Universität München, München, Germany; §Technische Universität München, Lehrstuhl für Biotechnologie der Nutztiere, Freising, Germany

Abstract

A placebo-controlled phase 3 trial demonstrated that the epidermal growth factor receptor (EGFR) inhibitor erlotinib in combination with gemcitabine was especially efficient in a pancreatic ductal adenocarcinoma (PDAC) subgroup of patients developing skin toxicity. However, EGFR expression was not predictive for response, and markers to characterize an erlotinib-responding PDAC group are currently missing. In this work, we observed high erlotinib IC_{50} values in a panel of human and murine PDAC cell lines. Using EGFR small interfering RNA, we detected that the erlotinib response was marginally influenced by EGFR. To find novel EGFR targets, we used an unbiased chemical proteomics approach for target identification and quality-controlled target affinity determination combined with quantitative mass spectrometry based on stable isotope labeling by amino acids in cell culture. In contrast to gefitinib, we observed a broad target profile of erlotinib in PDAC cells by quantitative proteomics. Six protein kinases bind to erlotinib with similar or higher affinity (K_d = 0.09-0.358 μM) than the EGFR (K_d 0.434 μM). We provide evidence that one of the novel erlotinib targets, ARG, contributes in part to the erlotinib response in a PDAC cell line. Our data show that erlotinib is a multikinase inhibitor, which can act independent of EGFR in PDAC. These findings may help to monitor future erlotinib trials in the clinic.

Neoplasia (2011) 13, 1026–1034

Introduction

The epidermal growth factor (EGF)/ErbB family of transmembrane tyrosine kinase growth factor receptors include the EGF receptor (EGFR/ErbB1), Her2/ErbB2, ErbB3, and ErbB4. Ligand-induced homodimeriziation or heterodimeriziation induces autophosphorylation of EGFR, recruitment of signaling intermediates, and activation of pathways such as Ras-ERK, phosphoinositide-3 kinase, Src, and STAT. Dysregulated expression and signaling of the EGFR, mediated by various mechanisms, is a common feature of solid cancers [1–3]. Several studies reported high expression of the EGFR, ranging from 7.7% to 100% of pancreatic ductal adenocarcinomas (PDACs) [4,

Address all correspondence to: Günter Schneider, MD, Technical University of Munich, Klinikum rechts der Isar, II. Medizinische Klinik, Ismaninger Str. 22, 81675 Munich, Germany. E-mail: guenter.schneider@lrz.tum.de

[1]This work was supported by the Bayerische Forschungsstiftung (AZ-845-08 to K.G., A.S., R.M.S., D.S., and G.S.), the Rudolf-Bartling Stiftung (Projekt IV/108 to G.S.), and the DFG (SFB824/C9 to D.S. and G.S.). The authors have declared that no competing interests exist.

[2]This article refers to supplementary materials, which are designated by Tables W1 W2 and are available online at www.neoplasia.com.

[3]These authors equally contributed to this study.

Received 19 July 2011; Revised 10 October 2011; Accepted 10 October 2011

DOI 10.1593/neo.111016

and, referent herein, therein]. Subsequently, the orally active small-molecule EGFR inhibitor erlotinib was the first drug approved by the US Food and Drug Administration for the treatment of advanced PDAC in combination with gemcitabine. The quinazolin derivative erlotinib (OSI-774) competes with ATP for binding to the catalytic domain of the EGFR, disrupting downstream signal transduction [5]. In a randomized, double-blind, placebo-controlled phase 3 trial, erlotinib plus gemcitabine was shown to be superior to gemcitabine monotherapy in patients with advanced or metastatic PDAC [6]. Although the median survival in the erlotinib plus gemcitabine arm (6.24 months) was only marginally better than gemcitabine monotherapy (5.91 months; hazard ratio = 0.82, $P = .038$), the combination was especially efficient in a subgroup of patients developing erlotinib-induced skin toxicity grade 2 or higher [6]. Despite the clear increase of the median survival in this particular subgroup to 10.5 months, EGFR expression levels were not predictors of response, arguing for the contribution of erlotinib off-targets.

Materials and Methods

Compounds

Erlotinib hydrochloride salt (Tarceva, OSI-774), imatinib methanesulfonate salt (Gleevec, STI-571), and gefitinib free base (Iressa, ZD1839) were purchased from LC Laboratories (Woburn, MA).

Generation and Culture of PDAC Cells

Primary dispersed murine pancreatic cancer cells were established from a genetically engineered $Kras^{G12D}$-based mouse model of pancreatic cancer and cultivated as recently described [7,8] (see Table W1 for a detailed description of the murine PDAC cells used). Primary dispersed human PDAC cells, Technical University Munich Pancreatic Cancer cells (TUM-PaCa3), were isolated from a primary PDAC (G2, pT4, pN1 [6/12]). Excess tumor tissue not needed for diagnostics from a surgically resected PDAC was placed into chilled sterile RPMI 1640 (HyClone, Logan, UT) supplemented with 1% (vol/vol) penicillin/streptomycin/amphotericin B (P/S/A; Invitrogen, Darmstadt, Germany). The tumor was washed twice, dissected into 1-mm cubes, and digested in RPMI 1640 medium supplemented with 15% fetal calf serum (Biochrome, Berlin, Germany), 1% (vol/vol) P/S/A, and 200 U/ml collagenase Type IV (Worthington Biochemical, Lakewood, NJ) at 37°C for 24 hours. Dispersed TUM-PaCa3 cells were subsequently pelleted by centrifugation and cultured in RPMI 1640 medium (15% fetal calf serum, 1% [vol/vol] P/S/A). Only low-passaged (passages 3 and 4) dispersed TUM-PaCa3 cells were used for assays. Use of tumor specimens was approved by the local ethical committee, and patients provided signed informed consent. Human pancreatic cancer cell lines were cultivated as recently described [9–11].

Small Interfering RNA Transfection and Cell Viability Assays

Small interfering RNA (siRNA) were transfected as recently described [12], and the following targeting sequences were used: human EGFR 5′ G G C A C G A G T A A C A A G C T C A 3′, murine EGFR 5′ C A G A G G A C A A C A T A G A T G A 3′, human ARG 5′ C G G T C A G T A T G G A G A G G T T 3′, murine ARG 5′ C T A C C A C T G T T G T C A A G T A 3′, and control siRNA 5′ C A G T C G C G T T T G C G A C T G G 3′. Cell viability was measured by 3-(4,5-dimethylthiazol-2-yl)-2,5-diphenyltetrazolium bromide (MTT) assays as described [8,9]. All data were obtained from at least three independent experiments performed in triplicate, and the results are presented as the mean and SEM.

Total Cell Lysates, Western Blots, and Immunoprecipitations

Whole-cell lysates were prepared, and Western blots were carried out as recently described [8,9]. The following antibodies were used: EGFR (sc-03), control IgG and ARG (sc-6356; Santa Cruz Biotechnology, Santa Cruz, CA), antiphosphotyrosine (clone 4G10; Millipore, Billerica, MA), and β-actin (Sigma-Aldrich, Munich, Germany). Western blots were performed using Odyssey Infrared Imaging System (LI-COR Biosciences, Bad Homburg, Germany) as described [8,9]. For immunoprecipitations (IPs), cells were lysed in RIPA buffer (150 mM NaCl, 1% IGEPAL CA-630, 0.5% sodium deoxycholate, 0.1% SDS, 50 mM Tris, pH 8, 0.1 mM phenylmethanesulfonylfluoride [PMSF]), and IPs were performed as recently described [11]. To quantify EGFR and ARG protein expression, the ratio of EGFR/β-actin and ARG/β-actin was determined using the Odyssey Infrared Imaging System, which assures measurements in the linear range. MiaPaCa2 cells served as a reference cell line, blotted on each membrane. The relative expression of EGFR and ARG was calculated by setting the EGFR/β-actin and ARG/β-actin ratio determined in MiaPaCa2 arbitrary to 1.

Compound Synthesis and Immobilization, In Vitro *Association Experiments, Mass Spectrometric Analysis, and Data Analysis*

Compound synthesis, stable isotope labeling by amino acids in cell culture (SILAC), *in vitro* association experiments and mass spectrometric analysis were reported [13–17] and described in detail in Supplemental Materials and Methods.

Statistical Methods

A two-tailed Student's *t* test was used to test statistical significance. *P* values are indicated and an asterisk (*) denotes a *P* value of less than .05. The half-maximal inhibitory concentration (IC_{50}) values were calculated with GraphPad Prism4 software (La Jolla, CA) using a nonlinear regression model with classic equations as described [9].

Results

To determine the sensitivity of primary murine and human PDAC cells and established human PDAC cell lines to erlotinib, the viability of cells treated with increasing concentrations of erlotinib (6, 12, and 18 μM) for 48 hours was measured in MTT assays to calculate the IC_{50}. Confirming recent observations [18–21] and compared with peak plasma levels measured in patients [22,23], we detected quite high IC_{50} values for erlotinib in human and murine PDAC cells; the most sensitive cells showed IC_{50} values greater than 10 μM (Figure 1*A* and Table 1). Mean IC_{50} values of murine cells, established from $Kras^{G12D}$-dependent PDACs, and established human PDAC cell lines were not significantly different (Figure 1*B*), indicating that primary dispersed low-passaged murine cell collections are a valid platform for the investigation of PDAC drug responses. Furthermore, low-passaged dispersed TUM-PaCa3 cells established from a primary human PDAC exhibits an IC_{50} in the range of established human PDAC cell lines, suggesting that the observed high IC_{50} values are not influenced by higher passage numbers and clonality of conventional human PDAC cell lines. Interestingly, the EGFR protein abundance was not correlated with the IC_{50} levels for erlotinib (Figure 1, *C* and *D*), arguing that erlotinib might act independent of EGFR.

To investigate the impact of the EGFR for pancreatic cancer cell viability and the therapeutic response toward erlotinib directly, we used an EGFR-specific siRNA. Whereas a slight decrease of cell viability on the EGFR knockdown was observed in MiaPaCa2 and

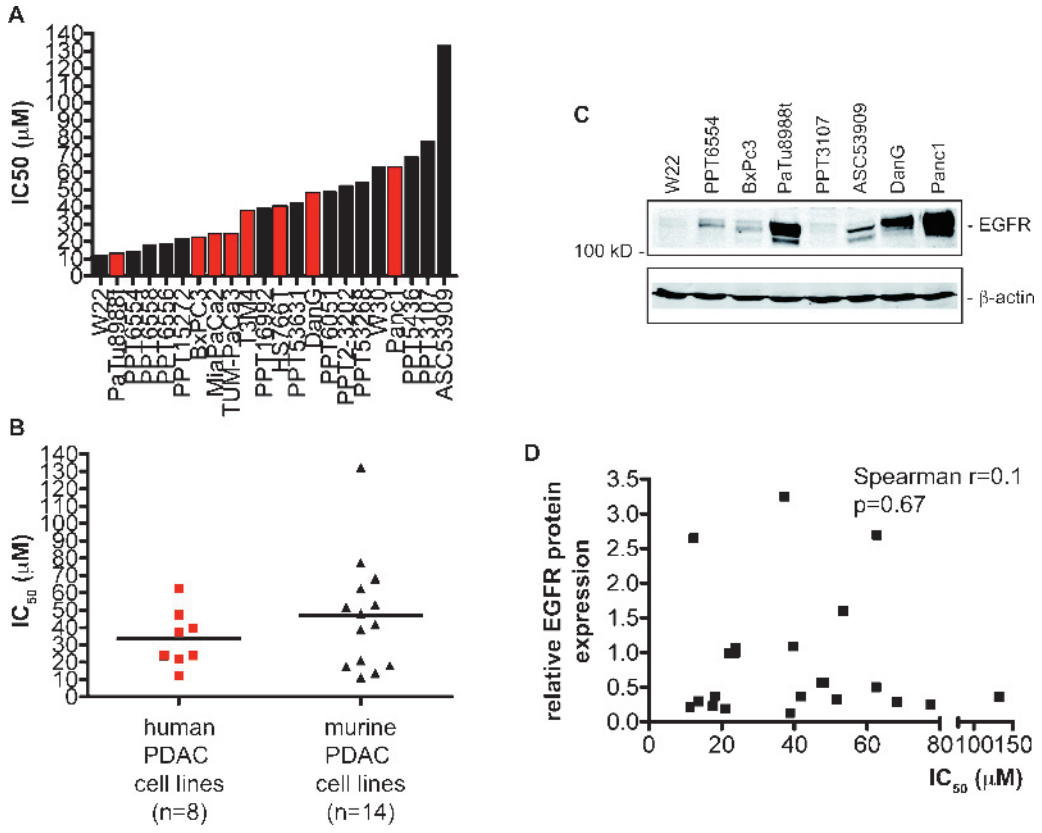

Figure 1. Erlotinib IC_{50} values of murine and human PDAC cells. (A) Viability of PDAC cells after treatment with 6, 12, and 18 μM erlotinib was measured by MTT assay and compared to vehicle-treated controls. IC_{50} values of murine (black) and human (red) PDAC cell lines were calculated using a nonlinear regression model. Statistics can be found in Table 1. (B) Mean IC_{50} values of murine (black triangle) and human (red square) PDAC cell lines show no statistically significant differences (Student's *t* test, $P = .15$). (C) Western blot analysis of EGFR expression levels in the indicated PDAC cell lines. β-Actin controls equal protein loading. (D) Correlation of the erlotinib IC_{50} values with EGFR protein expression levels in 22 PDAC cell lines. The Spearman correlation coefficient and the *P* value (two-tailed) are indicated.

BxPc3 cells, depletion of EGFR did not influence the viability of human T3M4 or murine PPT6554 cells (Figure 2, *middle panel*). Surprisingly, the erlotinib response was quite similar, irrespectively of EGFR depletion (Figure 2, *right panel*). Together, these data suggest that off-targets beyond EGFR may contribute to the erlotinib response in PDAC cells.

To find possible novel erlotinib targets, we used an unbiased chemical proteomics approach for target identification and quality-controlled target affinity determination using quantitative mass spectrometry based on SILAC [14]. Primary dispersed murine PPT6554 cells were used because it is one of the more erlotinib-sensitive lines. In the addition to some nonkinase proteins (Figure 3*A*, *green*), we identified several kinases (Figure 3*A*, *blue and purple*) and kinase-associated proteins (Figure 3*A*, *orange*) bound with high affinity by erlotinib. Importantly, six kinases, namely, the serine/threonine protein kinase 10 (STK10/LOK), the mitogen-activated protein kinase kinase kinase 1 (MAP3K1), the integrin-linked kinase (ILK), the STE20-like serine/threonine–protein kinase (SLK), the receptor-interacting serine/threonine–protein kinase 2 (Ripk2), and the tyrosine-protein kinase ARG (abelson-related gene; ABL2), revealed even higher binding affinity to erlotinib than EGFR (dissociation constant [K_d] = 0.434 μM). Here, K_d values ranging from 0.09 to 0.358 μM were determined, respectively (Figure 3*A*

Table 1. Response of Murine and Human PDAC Cell Lines to Erlotinib.

Cell Line	IC_{50} (48 h) (μM Erlotinib)	95% CI
Human PDAC cells		
PaTu8988t	12.3	9.9-15.4
BxPc3	21.9	17.1-28
MiaPaCa2	23.7	19.7-28.5
TUM-PaCa3	23.9	19.2-29.8
T3M4	37.3	29.7-46.9
HS766T	39.6	34.8-45
DanG	47.4	37-60.7
Panc1	62.6	53.3-72.1
Murine PDAC cells		
W22	11.3	10.1-12.7
PPT6554	13.7	11.8-15.8
PPT6558	17.6	15.8-19.6
PPT6556	18.1	13.6-24.3
PPT15272	21.0	17.2-25.7
PPT16992	38.8	32.2-46.8
PPT53631	41.7	30.9-56.2
PPT6051	48.1	34.8-66.5
PPT2-3202	51.6	36.9-72.3
PPT53268	53.3	29.1-97.9
W30	62.4	44.7-87
PPT5436	68.2	49.6-93.7
PPT3107	77.4	47.2-126.9
ASC53909	132.3	92.0-190.0

and Table W2). To compare the target profiles of different EGFR inhibitors, we performed the same experiment using the small-molecule EGFR inhibitor gefitinib, which binds with similar affinity to the EGFR (K_d = 0.323 μM) in PPT6554 cells (Figure 3*B*). Only one kinase, Ripk2 (K_d = 0.155 μM), was bound by gefitinib with a higher affinity than the EGFR. Whereas gefitinib binds only three kinases with a high affinity (K_d < 1 μM), erlotinib targets 11 protein kinases (Figure 3 and Table W2). These data clearly demonstrate that erlotinib is a multikinase

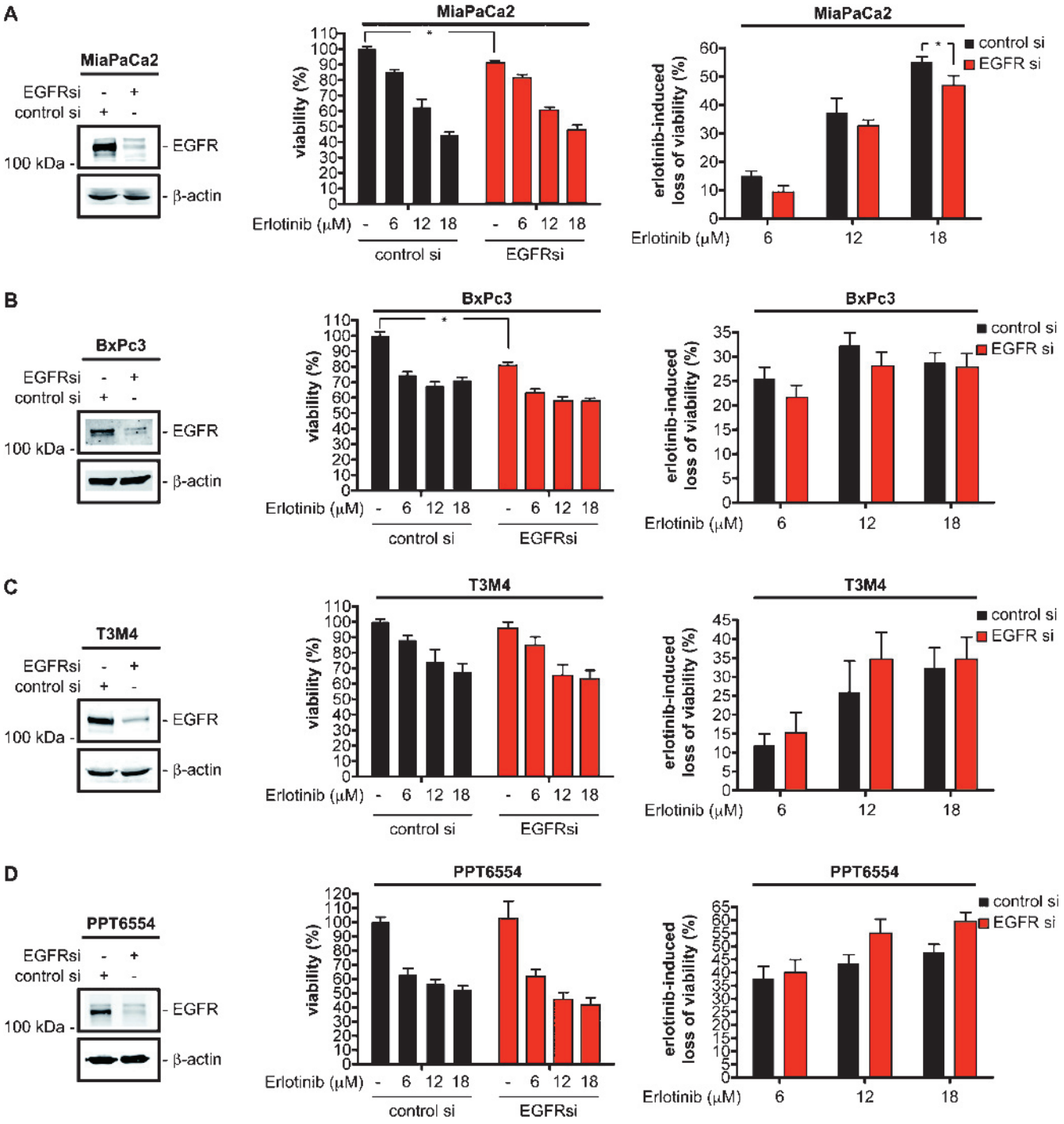

Figure 2. Erlotinib response of PDAC cells is EGFR independent. MiaPaCa2 (A), BxPc3 (B), T3M4 (C), and PPT6554 (D) cells were transfected with a control siRNA or an EGFR-specific siRNA. Left panel: Knockdown of the EGFR 48 hours after the transfection by Western blot analysis. β-Actin controls equal protein loading. Twenty-four hours after transfection, cells were treated with increasing doses of erlotinib as indicated for 48 hours or were left as an untreated control. Viability was determined using MTT assays. Middle panel: Viability of control siRNA-transfected cells was arbitrarily set to 100% and compared to (I) control siRNA-transfected and erlotinib-treated cells, to (II) EGFR siRNA-transfected cells, and to (III) EGFR siRNA-transfected and erlotinib-treated cells. Right panel: Erlotinib-induced therapeutic response in control and EGFR siRNA-transfected cells. Note that the right panels rely on an extrapolation of the data presented in the middle panels to better visualize the erlotinib-induced loss of viability (=therapeutic response) in control and EGFR siRNA-transfected cells. Student's *t* test, $^*P < .05$ *versus* controls.

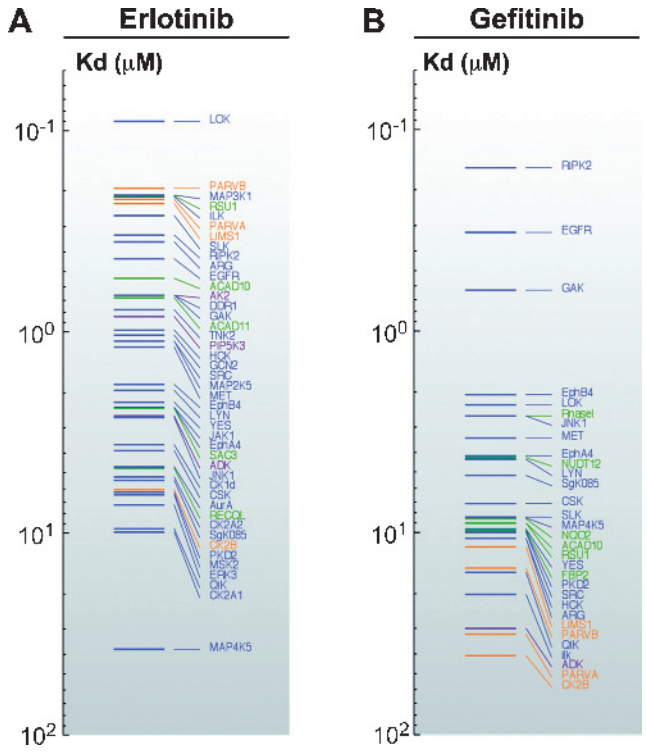

Figure 3. Target profiles of gefitinib and erlotinib. Shown are the target proteins of erlotinib (A) and gefitinib (B) in dispersed primary murine pancreatic cancer cells PPT6554. K_d values are plotted on a logarithmic scale, and target proteins are ranked from low (top) to high (bottom) K_d values. Protein kinases are depicted in blue; other kinases, purple; associated proteins, orange; and other proteins, green. Target proteins with K_d values lower than 10 μM are shown. In addition, target proteins with K_d values greater than 10 μM are indicated if they were identified as targets for both compounds. A complete list of all target proteins is provided in Table W2.

inhibitor in PDAC cells. A complete list of erlotinib and gefitinib targets, including sequence coverage, binding curves, competition curves, and K_d values, can be found in Table W2.

In excellent work using a patient-derived xenotransplant model, Jimeno et al. [19] described 25 genes defining a core enrichment gene set linked to EGFR inhibitor sensitivity. Because ARG was included in the gene set and was found to bind to erlotinib (Figure 3), we tested whether ARG was involved in the erlotinib response of pancreatic cancer cells. Knockdown of ARG resulted in a statistically significant loss of viability in human PDAC cells (Figure 4, *middle panel*). No change in viability after the ARG knockdown was observed in murine PPT6554 cells. Erlotinib responsiveness remained unchanged in BxPc3 and PPT6554 cells after ARG knockdown (Figure 4, *right panel*). In contrast, erlotinib evoked a distinct impaired response in T3M4 and MiaPaCa2 cells after ARG knockdown (Figure 4, *right panel*). Especially in T3M4 cells, the therapeutic response was ARG-dependent at low erlotinib concentrations, suggesting that ARG contributes to the erlotinib response in at least a subset of PDACs. The ARG kinase is activated by autophosphorylation at several sites [24]. We observed a reduced tyrosine phosphorylation of ARG in response to erlotinib in T3M4 cells (Figure 5*A*), which further confirms that ARG is targeted by erlotinib. However, ARG protein abundance was not correlated with IC_{50} values in the pancreatic cancer cell lines investigated (Figure 5, *B* and *C*), indicating that additional mechanisms and considerable high tumor heterogeneity exists in PDAC. Indeed, recent work shows that at least three distinct subtypes of PDAC exist with distinct clinicopathologic and molecular features [25].

ABL as well as ARG kinase activities were shown to be equally inhibited by imatinib [24]. However, T3M4 cells are not characterized by a particular imatinib sensitivity (Figure 5, *D*–*G*), which is consistent with the observation that only approximately 20% to 25% of the viability of T3M4 cells is controlled by ARG (Figure 4*C*).

Discussion

Recent sequence analysis of PDAC has uncovered mutations of genes in 12 core signaling pathways, demonstrating that PDAC is a genetically complex disease [26]. This complexity contributes to interindividual tumor heterogeneity and is reflected in the therapeutic effectiveness of the EGFR inhibitor erlotinib. Only a subset of patients responds to the erlotinib/gemcitabine combination therapy illustrating the need for markers to identify patients most likely to benefit from treatment. Currently, no such markers to predict response to erlotinib treatment in PDAC are available. Furthermore, the level of EGFR expression does not correlate with therapeutic response because the erlotinib/gemcitabine combination is equally efficient in patients who express EGFR as those who do not [6]. Consistently, EGFR amplification and response toward combined erlotinib/gemcitabine therapy were recently investigated using fluorescence *in situ* hybridization analysis and demonstrated no predictive value of EGFR amplifications [27]. These observations together with our data, demonstrating that the erlotinib response is marginally influenced by EGFR expression and that erlotinib IC_{50} values are not correlated with EGFR protein expression, argue that off-targets can contribute to therapeutic efficacy.

Using a proteome-wide unbiased approach for determining drug targets [14], we detected several kinases targeted by erlotinib in PDAC cells. STK10/LOK, MAP3K1, ILK, SLK, Ripk2, and ARG bind to erlotinib with higher affinity than EGFR. Consistently, STK10/LOK, SLK, RIPK2, and ARG were recently shown to bind to erlotinib in an *in vitro* competition binding assay [28]. To our knowledge, no data are currently available for expression or function of the STK10/LOK and SLK kinases in PDAC. Consistent with our observations, the tyrosine kinase activity of Ripk2 was recently shown to be inhibited by erlotinib and gefitinib [29]. Ripk2 is upstream of NFκB signaling, a pathway that can mediate proliferation and therapeutic resistance of PDAC cells [30]. However, detailed analysis of RipK2 function in PDAC is currently not available. High MAP3K1 expression was correlated with tumor differentiation and lymph node metastasis in PDAC [31]. Strong ILK expression is an independent prognostic factor in PDAC patients after resection [32]. From the therapeutic view, ILK was demonstrated to be involved in gemcitabine resistance of PDAC cells [33,34]. Increased transcript levels of ARG were described in approximately 30% of PDACs [35]. Therefore, erlotinib targets several kinases with well-documented expression and at least putative tumor-relevant functions in PDAC. It would follow that a patient subpopulation with tumors addicted to the expression of a kinase subset that is efficiently inhibited by erlotinib, the erlotinib target kinome, responds to therapy. Consistent with this, preclinical data from glioblastoma multiforme, which is like PDAC characterized by the activation of multiple core signaling pathways, including the EGFR-pathway [36,37], clearly demonstrate that several kinases must be efficiently targeted to inhibit survival signaling and to induce a potent therapeutic response [38]. In addition, a PDAC subset might exist, where survival of the tumor cells is critically dependent on the activity of one kinase.

Interestingly, we observed that the erlotinib response of human T3M4 cells toward a clinically more relevant dose of 6 μM erlotinib [22,23] depends in part on the presence of ARG. In addition to a wild-type *Kras* status [39], T3M4 cells have higher ARG messenger RNA levels than other human PDAC cell lines [35]. Furthermore, ARG is included in a gene set that defines EGFR inhibitor responsiveness of PDAC [19]. However, we observed no correlation of the ARG protein expression with the IC_{50} values of erlotinib in the 22 PDAC cell lines investigated, which is consistent with the known tumor heterogeneity of PDAC and argues that the dependency of the erlotinib response toward ARG is

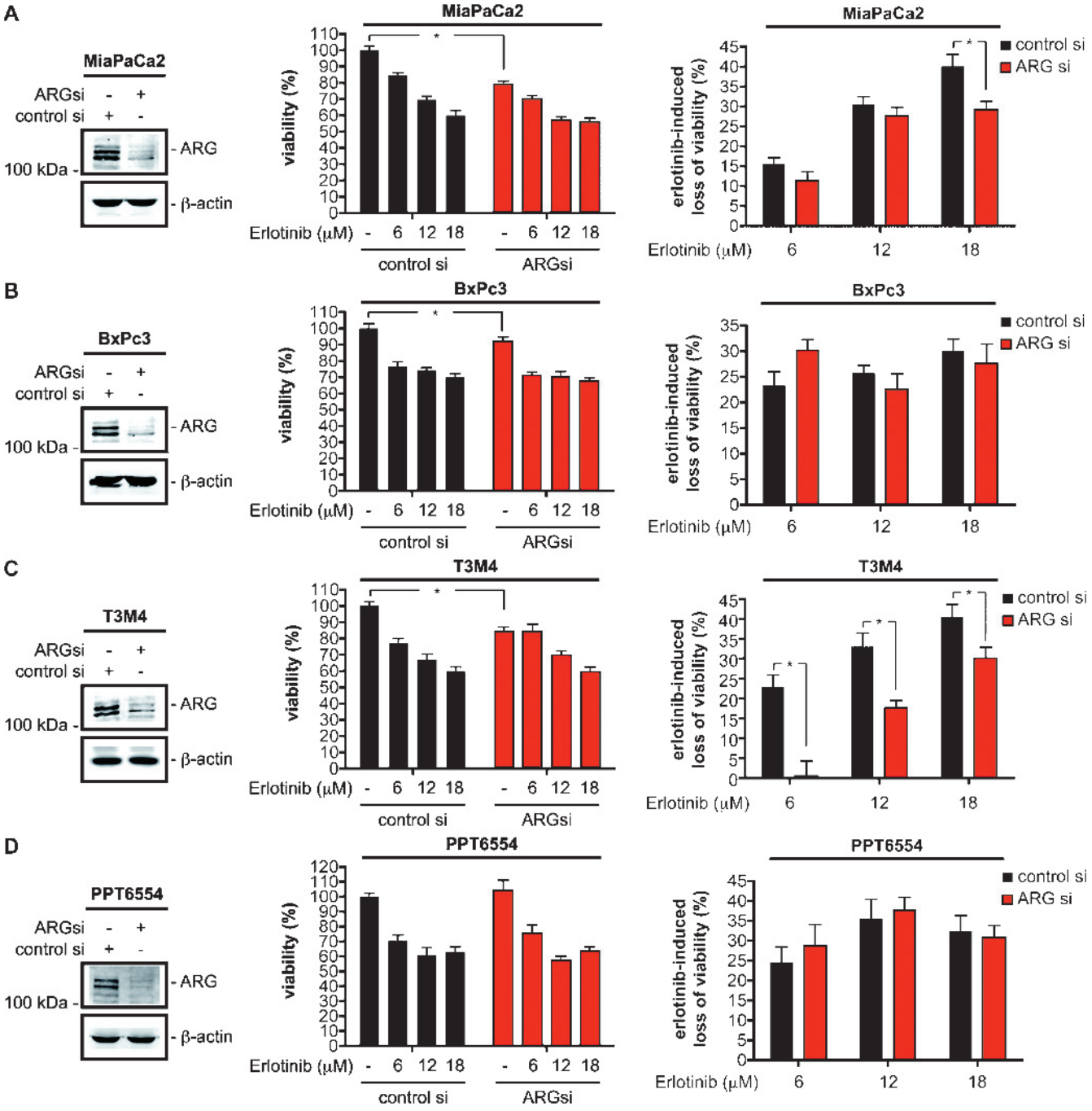

Figure 4. Role of ARG in the erlotinib response of PDAC cells. MiaPaCa2 (A), BxPc3 (B), T3M4 (C), and PPT6554 (D) cells were transfected with a control siRNA or an ARG-specific siRNA. Left panel: Knockdown of ARG 48 hours after the transfection by Western blot analysis. β-Actin controls equal protein loading. Twenty-four hours after transfection, cells were treated with increasing doses of erlotinib as indicated for 48 hours or were left as an untreated control. Viability was determined using MTT assays. Middle panel: Viability of control siRNA-transfected cells was arbitrarily set to 100% and compared to (I) control siRNA-transfected and erlotinib-treated cells, to (II) ARG siRNA-transfected cells, and to (III) ARG siRNA-transfected and erlotinib-treated cells. Right panel: Erlotinib-induced therapeutic response in control and ARG siRNA-transfected cells. Note that the right panels rely on an extrapolation of the data presented in the middle panels to better visualize the erlotinib-induced loss of viability (=therapeutic response) in control and ARG siRNA-transfected cells. Student's *t* test, $*P < .05$ *versus* controls.

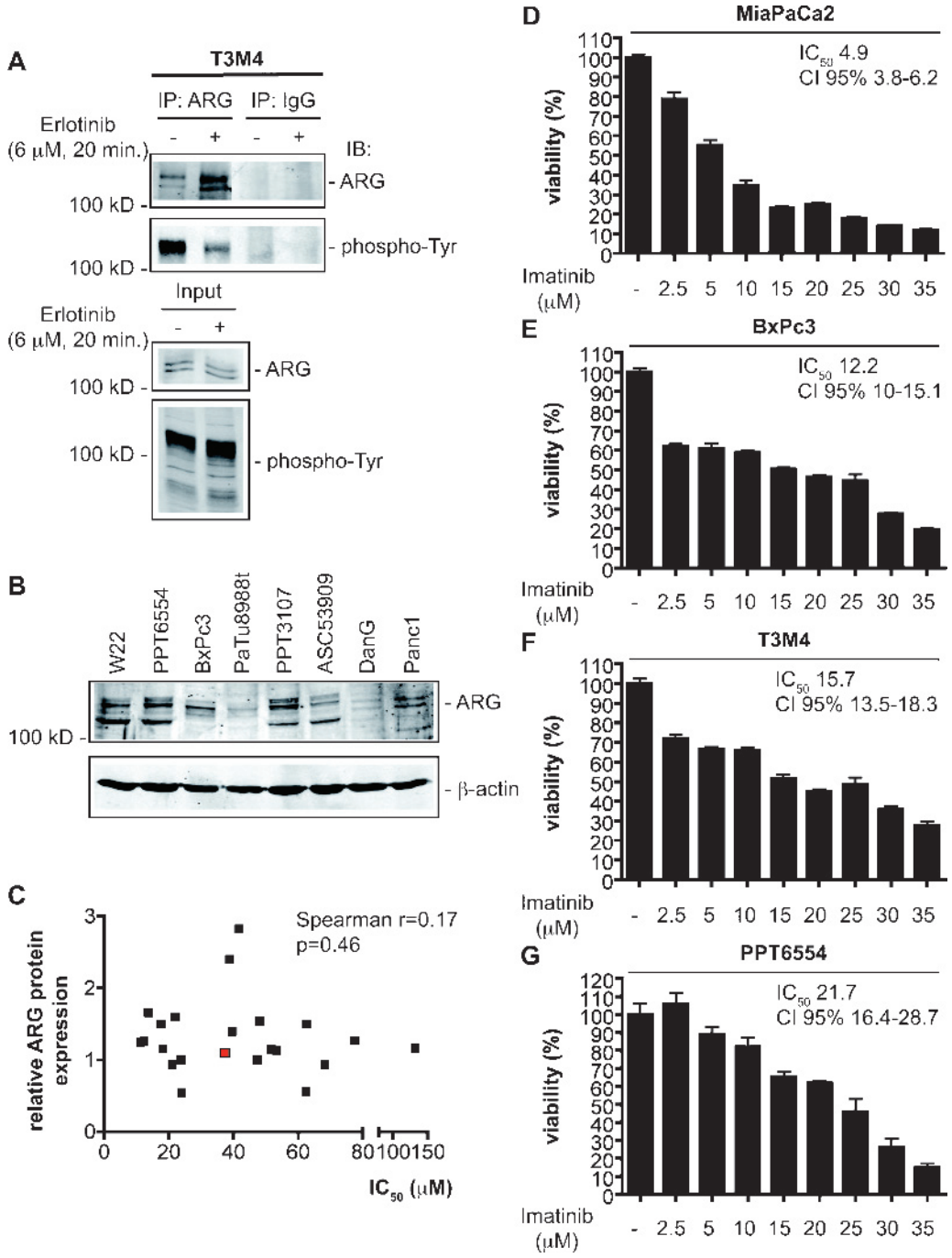

Figure 5. Tyrosine phosphorylation of ARG is reduced on erlotinib treatment. (A) T3M4 cells were treated with erlotinib as indicated or were left as an untreated control. After 20 minutes, whole-cell extracts were prepared, and ARG was immunoprecipitated. Pre–immune IgGs were used as precipitation controls. Western blots were performed with ARG and anti–phosphotyrosine antibodies. The input (5%) was probed with ARG and anti–phosphotyrosine antibodies. (B) Western blot analysis of ARG protein expression levels in the indicated PDAC cell lines. β-Actin controls equal protein loading. (C) Correlation of the erlotinib IC_{50} values with the ARG protein expression in 22 PDAC cell lines. The Spearman correlation coefficient and the *P* value (two-tailed) are indicated. T3M4 cells are depicted as a red box. MiaPaCa2 (D), BxPc3 (E), T3M4 (F), and PPT6554 (G) were treated with imatinib as indicated or with vehicle as control. Viability was determined after 48 hours using MTT assays. Imatinib IC_{50} values and the 95% confidence interval (95% CI) are indicated.

limited to a small PDAC subpopulation. Therefore, the contribution of ARG toward the erlotinib response in PDAC awaits further preclinical and clinical studies.

At the cellular level, ILK is located in focal adhesions, where the kinase is part of the ILK-pinch-parvin (IPP) complex. The IPP complex functions to connect integrins to the actin cytoskeleton and acts as a signaling hub to direct various processes, such as proliferation, motility, or invasion [40]. In addition to ILK, we detected the IPP components LIMS1 (PINCH1), parvin-α, and parvin-β recruited by erlotinib. However, the contribution of the IPP complex function in the erlotinib

response awaits further investigation. In addition, the impact of the nonprotein kinase proteins bound by erlotinib toward the erlotinib response is unclear now.

In addition to erlotinib, cetuximab, a monoclonal antibody directed against EGFR, was investigated in a large phase 3 trial in combination with gemcitabine in patients with locally advanced or metastatic PDAC [41]. Here and in contrast to the erlotinib/gemcitabine trial [6], no significant difference in median survival in the cetuximab/gemcitabine arm compared to gemcitabine monotherapy was observed [41]. Therefore, the erlotinib off-targets may explain the discrepant outcomes.

Consistent with our data, a recent report demonstrated that erlotinib, in contrast to gefitinib, potently inhibited STK10/LOK [42]. By inhibiting STK10/LOK, erlotinib can activate lymphocytes and exacerbate experimental skin inflammation *in vivo* [42]. Because lymphocytes are known to be involved in EGFR inhibitor–induced skin toxicity, the authors propose a contribution of STK10/LOK in this process [42]. Whether STK10/LOK or lymphocytes activated via STK10/LOK inhibition are involved in the therapeutic response on erlotinib treatment in human PDAC awaits further investigations.

In addition to the direct inhibition of erlotinib target kinases, rather indirect mechanisms can contribute to the sensitivity of PDAC cells toward erlotinib. For instance, erlotinib sensitivity of PDAC cells was recently shown to depend on the heterodimerization of the EGFR with ErbB3 [21]. However, the relevance of such mechanisms in clinical settings is unclear in the moment.

In summary, we demonstrate that erlotinib targets several kinases in PDAC with higher affinity than the EGFR and should therefore be considered as a multikinase inhibitor. We suggest two possibilities that characterize erlotinib responding PDAC cells: (I) high expression and/or functional relevance of a kinase subset efficiently inhibited by erlotinib or (II) addiction of the PDAC tumor cells to one kinase in the target spectrum of erlotinib. Whereas the relevance of these two possibilities in clinical settings is unclear at the moment and we cannot exclude the possibility that due to the wide heterogeneity of PDAC, none of the described erlotinib targets might predict erlotinib responsiveness. Our data may influence monitoring of future erlotinib trials to identify relevant erlotinib-responding subpopulations and to better stratify clinical trials and therapy.

Acknowledgments

The authors thank Monika Werb, Sandra Marx, and Vanessa Klein for excellent technical support and Priaxon AG for the synthesis and providing linker-erlotinib (KX214).

References

[1] Ray D, Ahsan A, Helman A, Chen G, Hegde A, Gurjar SR, Zhao L, Kiyokawa H, Beer DG, Lawrence TS, et al. (2011). Regulation of EGFR protein stability by the HECT-type ubiquitin ligase SMURF2. *Neoplasia* **13**, 570–578.

[2] Wakasaki T, Masuda M, Niiro H, Jabbarzadeh-Tabrizi S, Noda K, Taniyama T, Komune S, and Akashi K (2010). A critical role of c-Cbl–interacting protein of 85 kDa in the development and progression of head and neck squamous cell carcinomas through the *ras*-ERK pathway. *Neoplasia* **12**, 789–796.

[3] Avraham R and Yarden Y (2011). Feedback regulation of EGFR signalling: decision making by early and delayed loops. *Nat Rev Mol Cell Biol* **12**, 104–117.

[4] Bloomston M, Bhardwaj A, Ellison EC, and Frankel WL (2006). Epidermal growth factor receptor expression in pancreatic carcinoma using tissue microarray technique. *Dig Surg* **23**, 74–79.

[5] Grunwald V and Hidalgo M (2003). Developing inhibitors of the epidermal growth factor receptor for cancer treatment. *J Natl Cancer Inst* **95**, 851–867.

[6] Moore MJ, Goldstein D, Hamm J, Figer A, Hecht JR, Gallinger S, Au HJ, Murawa P, Walde D, Wolff RA, et al. (2007). Erlotinib plus gemcitabine compared with gemcitabine alone in patients with advanced pancreatic cancer: a phase III trial of the National Cancer Institute of Canada Clinical Trials Group. *J Clin Oncol* **25**, 1960–1966.

[7] von Burstin J, Eser S, Paul MC, Seidler B, Brandl M, Messer M, von Werder A, Schmidt A, Mages J, Pagel P, et al. (2009). E-cadherin regulates metastasis of pancreatic cancer *in vivo* and is suppressed by a SNAIL/HDAC1/HDAC2 repressor complex. *Gastroenterology* **137**, 361–371, 371.e1–371.e5.

[8] Schneider G, Henrich A, Greiner G, Wolf V, Lovas A, Wieczorek M, Wagner T, Reichardt S, von Werder A, Schmid RM, et al. (2010). Cross talk between stimulated NF-κB and the tumor suppressor p53. *Oncogene* **29**, 2795–2806.

[9] Fritsche P, Seidler B, Schüler S, Schnieke A, Göttlicher M, Schmid RM, Saur D, and Schneider G (2009). HDAC2 mediates therapeutic resistance of pancreatic cancer cells via the BH3-only protein NOXA. *Gut* **58**, 1399–1409.

[10] Retzer-Lidl M, Schmid RM, and Schneider G (2007). Inhibition of CDK4 impairs proliferation of pancreatic cancer cells and sensitizes towards TRAIL-induced apoptosis via downregulation of survivin. *Int J Cancer* **121**, 66–75.

[11] Schneider G, Saur D, Siveke JT, Fritsch R, Greten FR, and Schmid RM (2006). IKKα controls p52/RelB at the *skp2* gene promoter to regulate G_1- to S-phase progression. *EMBO J* **25**, 3801–3812.

[12] Wirth M, Fritsche P, Stojanovic N, Brandl M, Jaeckel S, Schmid RM, Saur D, and Schneider G (2011). A simple and cost-effective method to transfect small interfering RNAs into pancreatic cancer cell lines using polyethylenimine. *Pancreas* **40**, 144–150.

[13] Ong SE, Blagoev B, Kratchmarova I, Kristensen DB, Steen H, Pandey A, and Mann M (2002). Stable isotope labeling by amino acids in cell culture, SILAC, as a simple and accurate approach to expression proteomics. *Mol Cell Proteomics* **1**, 376–386.

[14] Sharma K, Weber C, Bairlein M, Greff Z, Keri G, Cox J, Olsen JV, and Daub H (2009). Proteomics strategy for quantitative protein interaction profiling in cell extracts. *Nat Methods* **6**, 741–744.

[15] Brehmer D, Greff Z, Godl K, Blencke S, Kurtenbach A, Weber M, Muller S, Klebl B, Cotten M, Keri G, et al. (2005). Cellular targets of gefitinib. *Cancer Res* **65**, 379–382.

[16] Cox J and Mann M (2008). MaxQuant enables high peptide identification rates, individualized p.p.b.-range mass accuracies and proteome-wide protein quantification. *Nat Biotechnol* **26**, 1367–1372.

[17] Cheng Y and Prusoff WH (1973). Relationship between the inhibition constant (K_1) and the concentration of inhibitor which causes 50 per cent inhibition (I_{50}) of an enzymatic reaction. *Biochem Pharmacol* **22**, 3099–3108.

[18] Buck E, Eyzaguirre A, Haley JD, Gibson NW, Cagnoni P, and Iwata KK (2006). Inactivation of Akt by the epidermal growth factor receptor inhibitor erlotinib is mediated by HER-3 in pancreatic and colorectal tumor cell lines and contributes to erlotinib sensitivity. *Mol Cancer Ther* **5**, 2051–2059.

[19] Jimeno A, Tan AC, Coffa J, Rajeshkumar NV, Kulesza P, Rubio-Viqueira B, Wheelhouse J, Diosdado B, Messersmith WA, Iacobuzio-Donahue C, et al. (2008). Coordinated epidermal growth factor receptor pathway gene overexpression predicts epidermal growth factor receptor inhibitor sensitivity in pancreatic cancer. *Cancer Res* **68**, 2841–2849.

[20] Tzeng CW, Frolov A, Frolova N, Jhala NC, Howard JH, Vickers SM, Buchsbaum DJ, Heslin MJ, and Arnoletti JP (2007). EGFR genomic gain and aberrant pathway signaling in pancreatic cancer patients. *J Surg Res* **143**, 20–26.

[21] Frolov A, Schuller K, Tzeng CW, Cannon EE, Ku BC, Howard JH, Vickers SM, Heslin MJ, Buchsbaum DJ, and Arnoletti JP (2007). ErbB3 expression and dimerization with EGFR influence pancreatic cancer cell sensitivity to erlotinib. *Cancer Biol Ther* **6**, 548–554.

[22] Tan AR, Yang X, Hewitt SM, Berman A, Lepper ER, Sparreboom A, Parr AL, Figg WD, Chow C, Steinberg SM, et al. (2004). Evaluation of biologic end points and pharmacokinetics in patients with metastatic breast cancer after treatment with erlotinib, an epidermal growth factor receptor tyrosine kinase inhibitor. *J Clin Oncol* **22**, 3080–3090.

[23] Hidalgo M, Siu LL, Nemunaitis J, Rizzo J, Hammond LA, Takimoto C, Eckhardt SG, Tolcher A, Britten CD, Denis L, et al. (2001). Phase I and pharmacologic study of OSI-774, an epidermal growth factor receptor tyrosine kinase inhibitor, in patients with advanced solid malignancies. *J Clin Oncol* **19**, 3267–3279.

[24] Tanis KQ, Veach D, Duewel HS, Bornmann WG, and Koleske AJ (2003). Two distinct phosphorylation pathways have additive effects on Abl family kinase activation. *Mol Cell Biol* **23**, 3884–3896.

[25] Collisson EA, Sadanandam A, Olson P, Gibb WJ, Truitt M, Gu S, Cooc J, Weinkle J, Kim GE, Jakkula L, et al. (2011). Subtypes of pancreatic ductal adenocarcinoma and their differing responses to therapy. *Nat Med* **17**, 500–503.

[26] Jones S, Zhang X, Parsons DW, Lin JC, Leary RJ, Angenendt P, Mankoo P, Carter H, Kamiyama H, Jimeno A, et al. (2008). Core signaling pathways in human pancreatic cancers revealed by global genomic analyses. *Science* **321**, 1801–1806.

[27] da Cunha Santos G, Dhani N, Tu D, Chin K, Ludkovski O, Kamel-Reid S, Squire J, Parulekar W, Moore MJ, and Tsao MS (2010). Molecular predictors of outcome in a phase 3 study of gemcitabine and erlotinib therapy in patients with advanced pancreatic cancer: National Cancer Institute of Canada Clinical Trials Group Study PA.3. *Cancer* **116**, 5599–5607.

[28] Karaman MW, Herrgard S, Treiber DK, Gallant P, Atteridge CE, Campbell BT, Chan KW, Ciceri P, Davis MI, Edeen PT, et al. (2008). A quantitative analysis of kinase inhibitor selectivity. *Nat Biotechnol* **26**, 127–132.

[29] Tigno-Aranjuez JT, Asara JM, and Abbott DW (2010). Inhibition of RIP2's tyrosine kinase activity limits NOD2-driven cytokine responses. *Genes Dev* **24**, 2666–2677.

[30] Sebens S, Arlt A, and Schäfer H (2008). NF-κB as a molecular target in the therapy of pancreatic carcinoma. *Recent Results Cancer Res* **177**, 151–164.

[31] Su F, Li H, Yan C, Jia B, Zhang Y, and Chen X (2009). Depleting MEKK1 expression inhibits the ability of invasion and migration of human pancreatic cancer cells. *J Cancer Res Clin Oncol* **135**, 1655–1663.

[32] Sawai H, Okada Y, Funahashi H, Matsuo Y, Takahashi H, Takeyama H, and Manabe T (2006). Integrin-linked kinase activity is associated with interleukin-1α–induced progressive behavior of pancreatic cancer and poor patient survival. *Oncogene* **25**, 3237–3246.

[33] Duxbury MS, Ito H, Benoit E, Waseem T, Ashley SW, and Whang EE (2005). RNA interference demonstrates a novel role for integrin-linked kinase as a determinant of pancreatic adenocarcinoma cell gemcitabine chemoresistance. *Clin Cancer Res* **11**, 3433–3438.

[34] Yau CY, Wheeler JJ, Sutton KL, and Hedley DW (2005). Inhibition of integrin-linked kinase by a selective small molecule inhibitor, QLT0254, inhibits the PI3K/PKB/mTOR, Stat3, and FKHR pathways and tumor growth, and enhances gemcitabine-induced apoptosis in human orthotopic primary pancreatic cancer xenografts. *Cancer Res* **65**, 1497–1504.

[35] Crnogorac-Jurcevic T, Efthimiou E, Nielsen T, Loader J, Terris B, Stamp G, Baron A, Scarpa A, and Lemoine NR (2002). Expression profiling of microdissected pancreatic adenocarcinomas. *Oncogene* **21**, 4587–4594.

[36] Hatanpaa KJ, Burma S, Zhao D, and Habib AA (2010). Epidermal growth factor receptor in glioma: signal transduction, neuropathology, imaging, and radioresistance. *Neoplasia* **12**, 675–684.

[37] Parsons DW, Jones S, Zhang X, Lin JC, Leary RJ, Angenendt P, Mankoo P, Carter H, Siu IM, Gallia GL, et al. (2008). An integrated genomic analysis of human glioblastoma multiforme. *Science* **321**, 1807–1812.

[38] Stommel JM, Kimmelman AC, Ying H, Nabioullin R, Ponugoti AH, Wiedemeyer R, Stegh AH, Bradner JE, Ligon KL, Brennan C, et al. (2007). Coactivation of receptor tyrosine kinases affects the response of tumor cells to targeted therapies. *Science* **318**, 287–290.

[39] Moore PS, Sipos B, Orlandini S, Sorio C, Real FX, Lemoine NR, Gress T, Bassi C, Kloppel G, Kalthoff H, et al. (2001). Genetic profile of 22 pancreatic carcinoma cell lines. Analysis of K-*ras*, p53, p16 and DPC4/Smad4. *Virchows Arch* **439**, 798–802.

[40] Cabodi S, del Pilar Camacho-Leal M, Di Stefano P, and Defilippi P (2010). Integrin signalling adaptors: not only figurants in the cancer story. *Nat Rev Cancer* **10**, 858–870.

[41] Philip PA, Benedetti J, Corless CL, Wong R, O'Reilly EM, Flynn PJ, Rowland KM, Atkins JN, Mirtsching BC, Rivkin SE, et al. (2010). Phase III study comparing gemcitabine plus cetuximab *versus* gemcitabine in patients with advanced pancreatic adenocarcinoma: Southwest Oncology Group-directed intergroup trial S0205. *J Clin Oncol* **28**, 3605–3610.

[42] Yamamoto N, Honma M, and Suzuki H (2011). Off-target serine/threonine kinase 10 inhibition by erlotinib enhances lymphocytic activity leading to severe skin disorders. *Mol Pharmacol* **80**, 466–475.

Supplemental Materials and Methods

Compound Synthesis and Immobilization

Erlotinib hydrochloride salt (Tarceva, OSI-774) and gefitinib free base (Iressa, ZD1839) were purchased from LC Laboratories (Woburn, MA). AX14596 (linker-gefitinib) was synthesized as described [1]. Synthesis of KX214 (6-amino-propoxy-linked 4-anilinoquinazoline) (linker-erlotinib):

The following schedule gives a short schematic overview about the synthetic route, which afforded the designated amino-propoxy–linked erlotinib-derivative **8**:

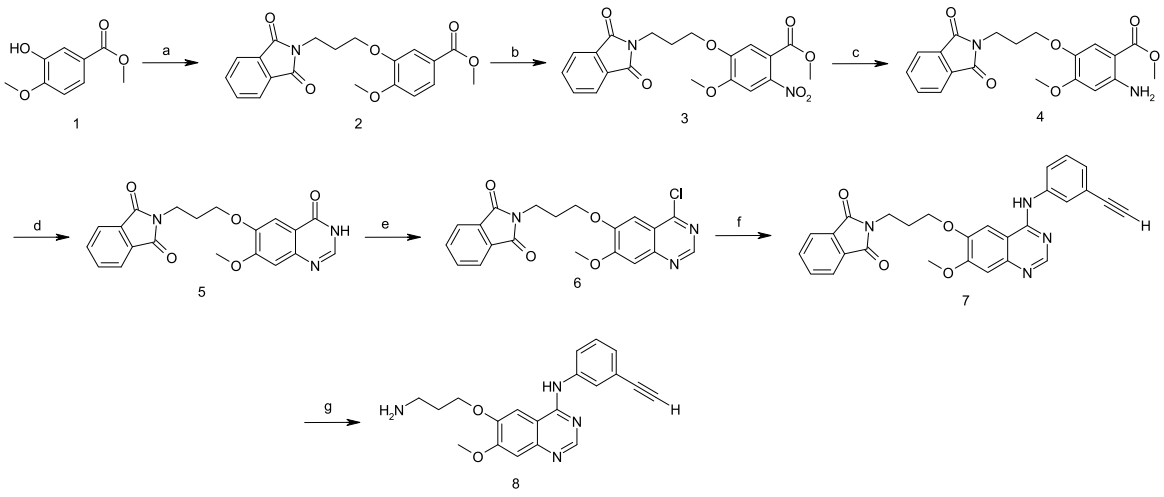

a) N -(3-bromopropyl)phthalimide, K_2CO_3, dimethylformamide (DMF), reflux; b) AcOH, HNO_3, H_2SO_4, room temperature; c) $SnCl_2$, ethyl acetate, H_2O, reflux; d) NH_4CHO_2, formamide, 140°C; e) $POCl_3$, *N*,*N*-dimethylaniline (DMA), 120°C; f) 3-aminophenylacetylene, chlorobenzene, 120°C; g) hydrazine hydrate, MeOH, room temperature.

The synthesis of compound **8** was performed by the application of a modified published synthetic procedure [2], starting with a base-promoted *O*-alkylation of methyl 3-hydroxy-4-methoxy-benzoate **1** with *N*-(3-bromopropyl)-phthalimide to give amino-protected intermediate **2**. Afterward, nitration and reduction of **2** afforded subsequently nitro-derivative **3** and methyl-2-amino-benzoate derivative **4**, respectively, and cyclization of **4** in the presence of formamide and ammonium formate yielded the key quinazoline-derivative **5**. Thereafter, **5** was treated with $POCl_3$ and a catalytical amount of *N*,*N*-dimethylaniline at 120°C and consecutive $S_{N,Ar}$ reaction with 3-aminophenylacetylene converted **6** to the amino-protected 4-anilinoquinazoline **7**. Finally, **7** underwent smoothly cleavage of the phthalimide functionality under basic conditions to release the free 6-amino-propoxy–linked 4-anilinoquinazoline **8**.

High-performance liquid chromatography–mass spectrometry (HPLC) and nuclear magnetic resonance spectroscopy (NMR) final analyses were performed with the following equipment and methods:

HPLC-MS.

Varian: 1200 L Triple Quadrupole mass spectrometer
Ionization mode: +ESI
UV-Detector: ProStar 325 (254 nm)
HPLC column: Varian Polaris C18 (length = 100 mm, diameter = 3 mm, particle size = 3 μm)
HPLC method:
Mobile phase: acetonitrile/water + 0.1% HCOOH
Run time: 9.50 minutes
Gradient: acetonitrile content was raised from 10% to 90% in 3 minutes

NMR.

Varian: Oxford NMR 400
^{1}H: 400.00 MHz
The samples were solved in $CDCl_3$ or dimethyl sulfoxide (DMSO)-d6.
Trimethylsilane was used as internal standard.

HPLC (preparative).

HPLC column: Varian RP Polaris C18 (length = 250 mm, diameter = 21.4 mm, particle size = 5 μm)
Mobile phase: acetonitrile/methanol + 0.1% HCOOH

*Synthesis of **2**.* A mixture of 0.2 g (0.0011 mol) of methyl 3-hydroxy-4-methoxy-benzoate, 0.45570 g (0.0017 mol) of *N*-(3-bromopropyl)-phthalimide, and 0.235 g (0.0017 mol) of sodium carbonate in 6 ml of DMF was stirred for 2 hours under reflux. The reaction mixture was

Table W1. Genotype of Murine Cell Lines.

Cell Line	Genotype
Murine PDAC cell lines	
W22	*Ptf1a$^{Cre/+}$;LSL-Kras$^{G12D/+}$;p53$^{loxP/lox}$;R26$^{LSL-TVA-LacZ/+}$*
PPT6554	*Ptf1a$^{Cre/+}$;LSL-Kras$^{G12D/+}$;p53$^{loxP/loxP}$;R26$^{LSL-TVA-LacZ/+}$*
PPT6556	*Ptf1a$^{Cre/+}$;LSL-Kras$^{G12D/+}$;p53$^{loxP/+;}$LSL-p53$^{R172H/+}$*
PPT6558	*Ptf1a$^{Cre/+}$;LSL-Kras$^{G12D/+}$;p53$^{loxP/+}$;LSL-p53$^{R172H/+}$;R26$^{LSL-TVA-LacZ/+}$*
W30	*Ptf1a$^{Cre/+}$;LSL-Kras$^{G12D/+}$;p53$^{loxP/+}$*
PPT15272	*Ptf1a$^{Cre/+}$;LSL-Kras$^{G12D/+}$*
PPT53268	*Ptf1a$^{Cre/+}$;LSL-Kras$^{G12D/+}$*
PPT16992	*Ptf1aCre/+;LSL-Kras$^{G12D/+}$;R26$^{LSL-TVA-LacZ/+}$*
PPT53631	*Ptf1a$^{Cre/+}$;LSL-Kras$^{G12D/+}$*
PPT6051	*PDX1-Cre;LSL-Kras$^{G12D/+}$;LSL-p53$^{R172H/+}$*
PPT3202	*Ptf1aCre/+;LSL-Kras$^{G12D/+}$;LSL-PCNA-Luc*
PPT5436	*Ptf1a$^{Cre/+}$;LSL-Kras$^{G12D/+}$;LSL-p53$^{R172H/R172H}$;R26$^{LSL-TVA-LacZ/LSL-TVA-LacZ}$*
PPT3107	*Ptf1a$^{Cre/+}$;LSL-Kras$^{G12D/+}$;LSL-p53$^{R172H/+}$;R26$^{LSL-TVA-LacZ/+}$*
ASC53909	*Ptf1a$^{Cre/+}$;LSL-Kras$^{G12D/+}$;R26$^{LSL-TVA-LacZ/+}$*

evaporated to dryness and the residue was dissolved in 20 ml of dichloromethane (DCM). The organic phase was washed with water and brine and finally dried over $MgSO_4$. Evaporation of the solvent under reduced pressure afforded the crude product, which was used for the following conversions without further purification.

Yield: 0.312 g (76.6%).

^{1}H NMR ($CDCl_3$, 400 MHz): 2.22–2.28 (m, 2H), 3.62 (s, 3H), 3.87 (s, 3H), 3.93 (t, ^3J = 8 Hz, 2H), 4.14 (t, ^3J = 2.4 Hz), 6.81 (d, ^3J = 4 Hz, 1H), 7.51 (d, ^4J = 2 Hz, 1H), 7.63–7.66 (m, 1H), 7.69–7.72 (m, 2H), 7.82–7.84 (m, 2H).

MS (ESI): m/z = 392 $[M + Na]^+$.

Synthesis of ***3****.* The amount of 10.56 ml of nitric acid and 12.31 ml of sulfuric acid at 0°C were dropwise added to a solution of 11,644 g (0.0315 mol) of **2** in 200 ml of acetic acid. After 1.5 hours of stirring at room temperature, the mixture was poured in 500 ml of H_2O at 0°C and extracted with 3 × 400 ml of DCM. The combined organic phases were washed with saturated Na_2CO_3(aq) and dried over $MgSO_4$. Evaporation of the solvent under reduced pressure afforded the crude product, which was used for the following conversions without further purification.

Yield: 10.48 g (80.2%).

^{1}H NMR ($CDCl_3$): 2.25–2.31 (m, 2H), 3.69 (s, 3H), 3.89 (s, 3H), 3.93 (t, ^3J = 6,4 Hz, 2H), 4.18 (t, ^3J = 5,6 Hz, 2H), 7.01 (s, 1H), 7.35 (s, 1H), 7.72–7.73 (m, 2H), 7.81–7.86 (m, 2H).

MS (ESI): m/z = 437 $[M + Na]^+$.

Synthesis of ***4****.* The amount 3.66 g (0,0193 mol) of tin chloride and 10 ml of water were subsequently added to a solution of 2 g (0.0048 mol) of **3** in 200 ml of ethyl acetate. After stirring for 1 hour under reflux, the heterogeneous mixture was diluted with 300 ml of ethyl acetate, and a resulting precipitate was removed by filtration. The organic phase was washed with saturated $NaHCO_3$(aq) and dried over $MgSO_4$. After removal of the solvent at reduced pressure, the desired product was purified and isolated by flash chromatography (silica, EE/H 1:1; 0.33).

Yield: 0.95 g (51.59%).

MS (ESI): m/z = 385 $[M + 1]^+$, 407 $[M + Na]^+$.

Synthesis of ***5****.* The amount of 0.237 g (0.0038 mol) of ammonium formate was added to a solution of 0.853 g (0.0022 mol) of **4** in 50 ml of formamide, and the mixture was stirred for 12 hours at 140°C. The reaction progress was monitored by HPLC, and after quantitative conversion, 100 ml of H_2O was poured to the organic solution, which conducted the formation of a beige precipitate. The solid was filtered off and washed subsequently with 50 ml of H_2O and 50 ml of ether. The isolated solid was dried in high vacuo, and the crude product was used in the following conversions without further purification.

Yield: 0.384 g (45.59%).

MS (ESI): m/z = 380 $[M + 1]^+$.

Synthesis of ***6****.* The amount of 1.93 ml (0,0027 mol) of *N*,*N*-dimethylaniline was dropwise added at 0°C to a solution of 2.127 g (0.0056 mol) of **5** in 10 ml of phosphorus oxychloride. After being stirred at room temperature for a further 5 minutes, the mixture was heated under reflux for additional 12 hours. Afterward, the mixture was poured into 50 ml of H_2O at 0°C, which induced precipitation of the demanded compound **6**. Filtration and washing with cold H_2O and finally with ether afforded compound **E** in satisfactory purity, and the crude product was used in the following conversions without further purification.

Yield: 1.77 g (79.53%).

MS (ESI): m/z = 398 $[M + 1]^+$.

Synthesis of ***7****.* A mixture of 1.774 g (0.0045 mol) of **6** and 0.783 g (0.0045 mol) of 3-aminophenylacetylene in 15 ml of chlorobenzene was stirred for 2 hours at 120°C. The maintaining precipitate was filtered off and subsequently washed with chlorobenzene, H_2O, and finally with ether. Removal of traces of solvent by high vacuo afforded the required compound **7**, which was applied in the following conversions without further purification.

Yield: 1.712 g (79.53%).

MS (ESI): m/z = 479 $[M + 1]^+$.

Synthesis of ***8****.* The amount of 0.020 g (0.0004 mol) g of hydrazine hydrate was added to a solution of 0.0654 g (0.00014 mol) of **7** in 4 ml of MeOH, and the mixture was stirred at ambient temperature. The reaction progress was monitored by HPLC, and after quantitative conversion, the reaction mixture was evaporated to dryness. The remaining residue was dissolved in 10 ml of DCM, washed with brine, and dried over $MgSO_4$. After removal of the solvent at reduced pressure, the product was purified by flash chromatography (silica, DCM/MeOH 4:1).

Yield: 20.7 mg (43.0%).

^{1}H NMR (D_2O): 2.19–2.22 (m, 2H), 3.30–3.31 (m, 2H), 3.51 (s, 1H), 3.98 (s, 3H), 4.30 (t, ^3J = 8,0 Hz, 2H), 7.10 (s, 1H), 7.23 (d, ^2J = 7,6 Hz, 1H), 7.35 (t, ^3J = 9,3 Hz, 1H), 7.68–7,77 (m, 2H), 7.87–8.0 (m, 1H), 8.41 (s, 1H).

MS (ESI): m/z = 349 $[M + 1]^+$.

For immobilization, drained epoxy-activated Sepharose 6B (GE Healthcare, Pittsburgh, PA) was resuspended in 2 volumes of 5 mM AX14596 or 5 mM linker-erlotinib dissolved in 50% DMSO/25 mM Na_2CO_3 and incubated with permanent agitation overnight at 30°C in the dark. Beads were washed with 50% DMSO/25 mM Na_2CO_3, and remaining active groups were blocked with 1 M ethanolamine. Subsequent washing steps were performed according to the manufacturer's instructions. To generate the control matrix, epoxy-activated Sepharose 6B was incubated with 1 M ethanolamine and treated as described above. The concentration of covalently immobilized inhibitor was determined spectrophotometrically by measuring the reduction of the inhibitor concentration in the soluble phase during the coupling reaction. EAH-Sepharose (GE Healthcare) was used as a negative control. The beads were stored at 4°C in the dark.

In Vitro *Association Experiments*

For SILAC, low-passaged (P4) primary dispersed murine pancreatic carcinoma cells from the primary PDAC of a *Ptf1a$^{Cre/+}$;LSL-Kras^{G12D};p53$^{lox/lox}$* mouse (#6554) (PPT6554) were cultivated as described previously [3,4]. For *in vitro* association experiments, PPT6554 cells were lysed in buffer containing 20 mM HEPES pH 7.5, 400 mM NaCl, 0.25% Triton X-100, 3 mM $MgCl_2$, 1 mM EDTA, 1 mM EGTA, 80 U/ml Benzonase plus additives (10 µg/ml aprotinin, 10 µg/ml leupeptin, 1 mM PMSF, 1 mM Na_3VO_4, 10 mM NaF). After centrifugation, lysates were adjusted to 1 M NaCl and filtered through a 0.45-µm cellulose acetate filter before *in vitro* association of 750 µl of lysate containing 3 mg of protein with either 30 µl of drained inhibitor

or control matrix for 2.5 hours at 4°C. Incubation procedures were performed essentially as described previously [4], with the addition that inhibitor beads representing five different compound densities were incubated with the cell extract to determine binding curves for each identified protein. For competition experiments, SILAC-encoded cell extracts were treated with different concentrations of erlotinib (0 nM, 10 nM, 100 nM, 300 nM, 1 μM, 10 μM, and 50 μM) or gefitinib (0 nM, 10 nM, 100 nM, 300 nM, 1 μM, 10 μM, and 100 μM) for 30 minutes before addition of inhibitor beads and incubation for an additional 2.5 hours at 4°C. In all *in vitro* association experiments, subsequent washing and elution steps including the separation of proteins by electrophoresis and the in-gel digest with trypsin were performed as described previously [4].

Mass Spectrometric Analysis

Mass spectrometric analysis of the labeled and combined peptide fractions was carried out by online nanoLC-MS/MS [4]. Samples were loaded directly by an Agilent 1200 nanoflow system (Agilent Technologies, Santa Clara, CA) on a 15-cm fused silica emitter (New Objective) packed in-house with reversed phase material (Reprusil-Pur C18-AQ, 3 μm; Dr. Maisch GmbH) at a flow of 500 nl/min. Bound peptides were eluted by a gradient from 2% to 40% solvent B (80% ACN and 0.5% HOAc) at a flow rate of 200 nl/min and sprayed directly into an LTQ-Orbitrap XL mass spectrometer (Thermo Fischer Scientific, Waltham, MA) at a spray voltage of 2 kV using a nanoelectrospray ion source (Proxeon Biosystems, Dreieich, Germany). The mass spectrometer was operated in the positive ion mode and a data-dependent switch between MS and MS/MS acquisition. To improve mass accuracy in the MS mode, the lock-mass option was enabled [5]. Full scans were acquired in the Orbitrap at a resolution $R = 60\,000$ and a target value of 1,000,000 charges. The five most intense ions detected in the MS were selected for collision-induced dissociation at a target value of 5000, and the resulting fragmentation spectra were recorded in the linear ion trap. Ions that were once selected for data-dependent acquisition were dynamically excluded for 30 seconds for further fragmentation.

Data Analysis

Mass spectra were processed using the MaxQuant software version 1.0.12.28 [6], using the Mascot search engine (version 2.2.0) for peptide and protein identification. A concatenated forward and reversed IPI mouse database (version 3.39) was used comprising 106,658 database entries. Regarding the search parameters, the minimal peptide length was set to six amino acids, trypsin was selected as the proteolytic enzyme, and maximally two missed cleavage sites were allowed. Carbamidomethylation of cysteine residues was selected as a fixed modification, whereas methionine oxidation and N-terminal protein acetylation were allowed as a variable modification. Because MaxQuant automatically extracts isotopic SILAC peptide triplets, the corresponding isotopic forms of lysine and arginine were automatically selected for database search as fixed modifications. The maximal mass deviation of precursor and fragment masses was set to 7 ppm and 0.5 Da. A false discovery rate of 0.01 was selected for proteins and peptides, and a posterior error probability (PEP) below or equal to 0.1 for each MS/MS spectrum was required. Target-specific dissociation constants for the tested free kinase inhibitors were calculated based on SILAC quantification data using the Cheng-Prusoff equation as described previously [7].

References

[1] Brehmer D, Greff Z, Godl K, Blencke S, Kurtenbach A, Weber M, Muller S, Klebl B, Cotten M, Keri G, et al. (2005). Cellular targets of gefitinib. *Cancer Res* **65**, 379–382.

[2] Knesl P, Roseling D, and Jordis U (2006). Improved synthesis of substituted 6,7-dihydroxy-4-quinazolineamines: tandutinib, erlotinib and gefitinib. *Molecules* **11**, 286–297.

[3] Ong SE, Blagoev B, Kratchmarova I, Kristensen DB, Steen H, Pandey A, and Mann M (2002). Stable isotope labeling by amino acids in cell culture, SILAC, as a simple and accurate approach to expression proteomics. *Mol Cell Proteomics* **1**, 376–386.

[4] Sharma K, Weber C, Bairlein M, Greff Z, Keri G, Cox J, Olsen JV, and Daub H (2009). Proteomics strategy for quantitative protein interaction profiling in cell extracts. *Nat Methods* **6**, 741–744.

[5] Olsen JV, de Godoy LM, Li G, Macek B, Mortensen P, Pesch R, Makarov A, Lange O, Horning S, and Mann M (2005). Parts per million mass accuracy on an Orbitrap mass spectrometer via lock mass injection into a C-trap. *Mol Cell Proteomics* **4**, 2010–2021.

[6] Cox J and Mann M (2008). MaxQuant enables high peptide identification rates, individualized p.p.b.-range mass accuracies and proteome-wide protein quantification. *Nat Biotechnol* **26**, 1367–1372.

[7] Cheng Y and Prusoff WH (1973). Relationship between the inhibition constant (K_1) and the concentration of inhibitor which causes 50 per cent inhibition (I_{50}) of an enzymatic reaction. *Biochem Pharmacol* **22**, 3099–3108.